

EasyNet: An Easy Network for 3D Industrial Anomaly Detection

Ruitao Chen*
Southern University of Science and
Technology
Shenzhen, China
chenrt2022@mail.sustech.edu.cn

Guoyang Xie*
Southern University of Science and
Technology
Shenzhen, China
University of Surrey
Guildford GU2 7XH, UK
guoyang.xie@surrey.ac.uk

Jiaqi Liu*
Southern University of Science and
Technology
Shenzhen, China
liujq32021@mail.sustech.edu.cn

Jinbao Wang†
Southern University of Science and
Technology
Shenzhen, China
linkingring@163.com

Ziqi Luo
Southern University of Science and
Technology
Shenzhen, China
12233217@mail.sustech.edu.cn

Jinfan Wang
Southern University of Science and
Technology
Shenzhen, China
wangjf@sustech.edu.cn

Feng Zheng†
CSE and RITAS, Southern University
of Science and Technology
Shenzhen, China
f.zheng@ieee.org

ABSTRACT

3D anomaly detection is an emerging and vital computer vision task in industrial manufacturing (IM). Recently many advanced algorithms have been published, but most of them cannot meet the needs of IM. There are several disadvantages: i) difficult to deploy on production lines since their algorithms heavily rely on large pre-trained models; ii) hugely increase storage overhead due to overuse of memory banks; iii) the inference speed cannot be achieved in real-time. To overcome these issues, we propose an easy and deployment-friendly network (called EasyNet) without using pre-trained models and memory banks: firstly, we design a multi-scale multi-modality feature encoder-decoder to accurately reconstruct the segmentation maps of anomalous regions and encourage the interaction between RGB images and depth images; secondly, we adopt a multi-modality anomaly segmentation network to achieve a precise anomaly map; thirdly, we propose an attention-based information entropy fusion module for feature fusion during inference, making it suitable for real-time deployment. Extensive experiments show that EasyNet achieves an anomaly detection AUROC of 92.6% without using pre-trained models and memory banks. In addition, EasyNet is faster than existing methods, with a high frame rate of 94.55 FPS on a Tesla V100 GPU.

KEYWORDS

3D anomaly detection, multi-modality fusion, unsupervised learning, industrial manufacturing

1 INTRODUCTION

There is a strong need to propose a deployment-friendly 3D unsupervised anomaly detection (3D-AD) model to tap the gap,

which brings 3D-AD’s capabilities into the factory floor. Currently, most of anomaly detection methods [21, 23, 35, 36] are based on 2D images. But in the quality inspection of industrial products, human inspectors utilize both color (RGB) characteristics and depth information to determine whether it is a defective product, where depth information is essential for anomaly detection. As shown in Figure 2, for foam and peach, it is difficult to identify the anomalies from the RGB image alone. Though 3D-AD algorithms [7, 29, 33] are attracting interest from the academy, most of them are far from satisfactory for industrial manufacturing (IM). According to Figure 1, there are several issues: i) The cutting-edge 3D-AD methods steadily rely on the representational abilities of large pre-trained models, leading to slow inference speed and huge storage overhead. ii) Feature embedding-based 3D-AD methods excessively use memory banks, leading to huge memory bank costs in real-world applications. Because of this, it is important and urgent to build an application-oriented 3D-AD model to meet the demands of IM.

To avoid using large pre-trained models and memory banks, we propose an easy but effective multi-modality anomaly detection and localization network, called **EasyNet**. Specifically, EasyNet consists of two parts, the Multi-modality Reconstruction Network (MRN) and the Multi-modality Segmentation Network (MSN). First, instead of directly using pre-trained features, we generate synthesized anomalies on RGB images and depth images and reconstruct the anomalies with semantically plausible free contents, while keeping the non-anomalous region of the multi-modality inputs (RGB images and depth images) unchanged. Simultaneously, to simplify the anomalous detection procedure by memory bank-based methods, we feed the reconstructed RGB image and depth image into a simple MSN to obtain the anomaly map. As shown in Figure 3, the whole architecture, including both MRN and MSN, significantly encourage the interaction between RGB and depth features.

*Equally contribute to this work

†Corresponding author

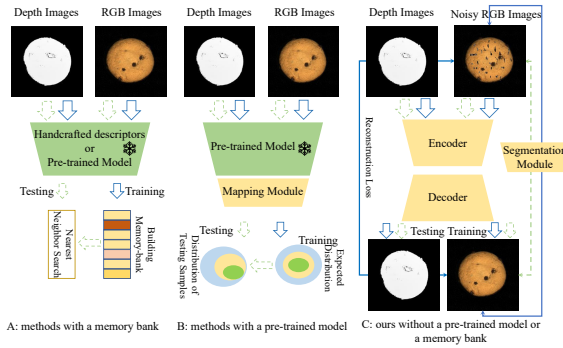


Figure 1: Illustration of 3D anomaly detection paradigms, including (A) feature embedding-based memory bank, (B) pre-trained network, and (C) encoder-decoder (ours).

To reduce the disturbance between RGB and depth images, we propose an efficient information entropy-based feature fusion scheme. We find that some 3D-AD methods, like AST [30] and BTF [17] cannot fully utilize the advantage of multi-modality fusion, i.e. RGB-D performance is not competitive than RGB performance. The main reason is that there are no uniform abnormal patterns in RGB or depth images. For example, some anomalies can be detected by pure RGB images and depth information works as the noise and may degrade the overall anomaly detection performance. While certain types of anomalies can be easily detected by depth images, RGB and depth feature fusion can greatly enhance anomaly detection performance. Hence, we propose a dynamic multi-modality fusion scheme to make use of RGB and depth features. The architecture of the fusion scheme is shown in Figure 5. Moreover, as shown in Table 5, our proposed fusion scheme is simple and much more computationally efficient than the aforementioned 3D-AD models [17, 30, 33]. Our proposed information entropy-based fusion scheme is easy to train and apply, with outstanding performance and inference speed. As a result, EasyNet can achieve 92.6% on MVTEC 3D-AD and 86.9% on Eyescandies in I-AUROC while running at 94.55 FPS, surpassing the previous best-published 3D-AD methods on accuracy and efficiency.

Our contributions can be summarized as follows:

- EasyNet is easy to implement and deploy for 3D unsupervised anomaly detection, i.e., eliminating the usage of pre-trained models and memory banks.
- We propose an Attention-based Information Fusion Module that achieves the fastest inference speed than the existing methods, with a high frame rate of 94.55 FPS on a Tesla V100 GPU.
- We present a Multi-modality Reconstruction Network(MRN) to accurately reconstruct the anomalous region and encourage the interaction of RGB and depth.
- We propose a Multi-modality Segmentation Network(MSN) to output the anomaly map precisely.
- EasyNet obtains the state-of-the-art result in Pure RGB. Note that EasyNet obtains the best anomaly detection AUROC of 92.6%, reducing the error by 40% compared to the next best performing.

2 RELATED WORK

Anomaly detection (AD) is a classical topic, which aims to distinguish normal samples and abnormal samples. Existing experimental settings usually only take normal samples as the training set, and evaluate the ability of the model to distinguish abnormal samples in the test set. The current unsupervised AD can be mainly divided into feature extraction-based methods and image reconstruction-based methods. The former is restricted by the pre-trained model, while the latter is free from this limitation. Based on this idea, we designed a reconstructive AD algorithm for RGB-D data, removing the restrictions on pre-trained models and memory banks.

2.1 2D Anomaly Detection

Since the emergence of the MVTEC AD dataset [4], research on AD in industrial 2D images has received more attention. Most existing research is based on this set for unsupervised AD tasks.

There is more research on feature embedding-based methods than reconstruction-based methods. The most basic idea is to regard AD as a one-class classification problem and turn the AD problem into a problem of finding boundaries for classification. CutPaste [20] and SimpleNet [24] are representative methods. They make abnormal samples and change unsupervised AD datasets into supervised datasets. Teacher-student architecture is another useful approach. The teacher network distills knowledge to the student network by extracting features from normal samples. While the teacher network and the student network perform differently when producing abnormal samples and they detect anomalies through this characteristic [5, 14]. Normalizing flow methods map samples into a Gaussian distribution, while abnormal samples deviate from this distribution [15, 28]. Methods based on memory banks are simple but effective, whose ideas come from the k-nearest neighbors (KNN) algorithm. They store features of normal samples and calculate the distance between the features of test samples and features of normal samples during testing to determine whether the samples are abnormal [13, 26]. As for reconstruction-based methods, most of them are similar in structure. They synthesize abnormal samples and restore abnormal samples to normal samples. For example, DRAEM [39] and NSA [31] synthesize abnormal samples in image level, while DSR [41] and UniAD [37] synthesize abnormal samples in feature level.

Generally, most of the 2D-AD methods use the pre-trained model of natural images to extract RGB’s features while they don’t process depth information, so it is difficult to apply to 3D-AD directly. There is a certain gap between the two, and our method tries to get rid of this dependence so that 2D-AD can smoothly transition to 3D-AD.

2.2 3D Anomaly Detection

Different from 2D-AD, 3D-AD is a new research topic since the publication of MVTEC 3D-AD [6]. As shown in Figure 2, 3D-AD is a more challenging but also more promising research direction. The effective use of depth information can greatly improve detection accuracy in specific scenarios. On the other hand, how to integrate depth information and prevent it from interfering with RGB information is the current difficulty.

Bergmann *et al.* [7] introduce a point cloud feature extraction network of the teacher-student model. During training, the features

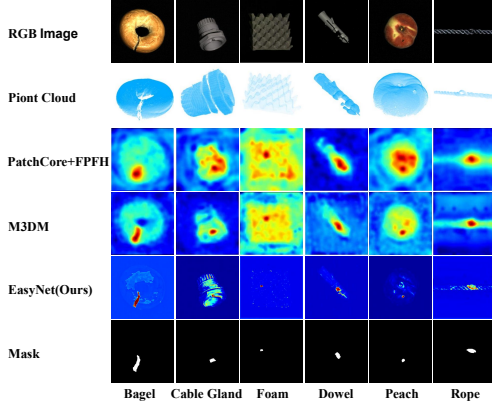


Figure 2: Simple examples of 3D anomaly detection on MVTec 3D-AD [6]. The first and second rows are made up of RGB and point clouds, respectively. The third to fifth rows show predicted outcomes of PatchCore+FPFH [18], M3DM [33], and EasyNet (ours), respectively. Mask refers to the anomaly region of a sample.

extracted by the student network and the teacher network are forced to be consistent. During the test, the differences between the features extracted by the teacher-student model are compared to locate anomalies. Horwitz *et al.* [17] combine hand-crafted 3D descriptors with the KNN framework, a classic AD approach. Those two methods are efficient but with poor performance. AST [29] gets a better result in MVTec 3D-AD. However, it only uses depth information to remove the background. AST still uses the 2D-AD method to detect anomalies and the depth information about items is ignored. Similar to BTF, but M3DM [33] extracts features from the point cloud and RGB images respectively and fuses them to make a decision, which has a better performance than treating RGB and depth as six-layer images as BTF. The visualization effect of M3DM is given in the fourth row of Figure 2. CPMF [10] also adopts the KNN paradigm, the difference is that the author projects the point cloud into 2D images from different angles, and fuses the obtained 2D image information for detection.

To summarize, the existing 3D-AD models either have poor performance or are greatly affected by pre-trained models and memory banks. Differently, we design a simple and effective 3D-AD model without relying on pre-trained models and memory banks. Our method achieves the SOTA performance outperforming all previous methods that learn without additional pre-training.

3 APPROACH

3.1 Problem Definition and Challenges

Our 3D-AD setting is similar to M3DM [33] and AST [30] and can be formally stated as follows. Given a set of training examples $\mathcal{T} = \{t_i\}_{i=1}^N$, in which $\{t_1, t_2, \dots, t_N\}$ are the normal samples and each of them consists of a paired images, RGB image I_{rgb} and depth image I_{depth} . In addition, \mathcal{T}_n belongs to one certain category, c_j , $c_j \in \mathcal{C}$, where \mathcal{C} denotes the set of all categories. During test time, given a normal or abnormal sample from a target category

c_j , the AD model should predict whether or not the test 3D object is anomalous and localize the anomaly region if the prediction result is anomalous. The following are the main challenges. (1) Less information on normal samples can be used. Each category’s training dataset contains only normal samples, i.e., no pixel-level annotations of I_{rgb} and I_{depth} . (2) It is difficult to find an effectively multi-modality fusion way. Because anomalies may appear in RGB, depth or in both. If we simply fuse both of these features, it may degrade the overall AD performance. (3) Real-world applications have limited storage space. So it is impractical to build a model that uses large pre-trained models and memory banks.

3.2 EasyNet

This section provides a comprehensive description of EasyNet. As illustrated in Figure 3, the proposed model comprises a multi-scale Multi-modality Reconstruction Network (MRN), a multi-scale Multi-modality Segmentation Network (MSN) and an attention-based information entropy fusion module, with the fusion network being exclusively applied during reasoning stages. The subsequent sections elaborate on the design and functionality of each module.

3.2.1 Multi-modality Reconstruction Network (MRN). The multi-modal reconstruction network establishes a task of image reconstruction. In this task, the network reconstructs the original image from an artificially corrupted image obtained from the simulator. The network is designed as an encoder-decoder structure to transform the local features of the input image into a mode that more closely resembles the normal sample distribution.

The framework of the simulator is depicted in Figure 4. We generate a foreground mask on the original depth image and apply a mask operation on the randomly generated Berlin noise figure. Our empirical evaluation reveals that only adding foreground noise exclusively assists the network in recognizing the noise on the foreground object rapidly. Next, the Berlin noise map undergoes binarization to produce positive and negative mask maps. Both random and original RGB images undergo weighting, alongside the Berlin noise map and depth image. Finally, the resulting outputs include RGB and depth images with anomalies and masks. Traditionally, the L_2 loss function is used in image reconstruction tasks, but it ignores the differences in structure and perception, resulting in the lack of spatial variation and multi-scale characteristics of the reconstructed images. The use of SSIM loss function (1) can not be a problem, so we use L_2 loss function and SSIM loss function in the reconstruction of network RGB images. In our experiment, it is also found that spatial variation and multi-scale features have limited and even negative effects on depth images, so only L_2 loss function is used in depth image reconstruction. We have:

$$L_{SSIM}(I, I_r) = \frac{1}{N_p} \sum_{i=1}^H \sum_{j=1}^W 1 - SSIM(I, I_r)_{(i,j)}, \quad (1)$$

where H and W are the height and width of image I , respectively. N_p equals the number of pixels in I . I_r represents the reconstruction output of the network.

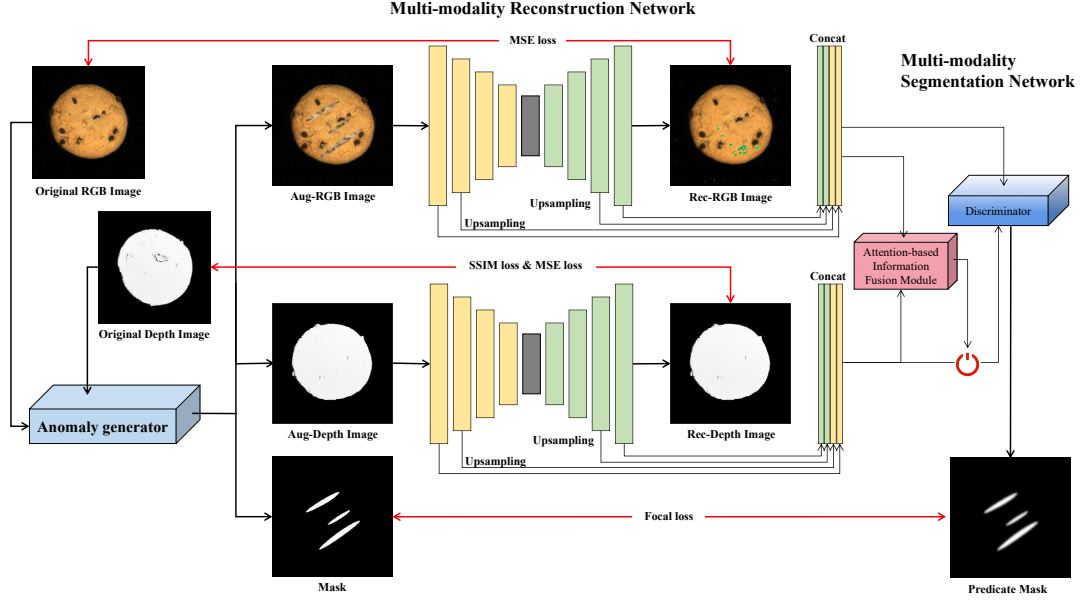


Figure 3: Total architecture of EasyNet. Our EasyNet consists of three main components. (1) Anomaly Generator adds Berlin noise to the original multi-modal images to simulate abnormal positive and negative enhanced RGB and depth images. (2) Multi-modality Reconstruction Network (MRN) constructs a reconstruction task to restore the enhanced anomaly images to RGB and depth images without anomalies while obtaining multi-modal feature information from multiple layers, where using two layers is used as an example. (3) The Multi-modality Segmentation Network (MSN) utilizes an attention-based information entropy fusion module to fuse the extracted multi-modal features. During training, the attention-based information entropy fusion module is fully open and taking control of feature flow during inference, it calculates the self-attention information entropy score for feature information from multiple modes to guide the network in integrating feature information. For the reconstruction task, we use SSIM loss [34] and MSE loss to calculate the reconstruction loss for RGB images, while only using MSE loss for depth images. Moreover, Focal loss[22] is used to calculate the pixel classification task loss.

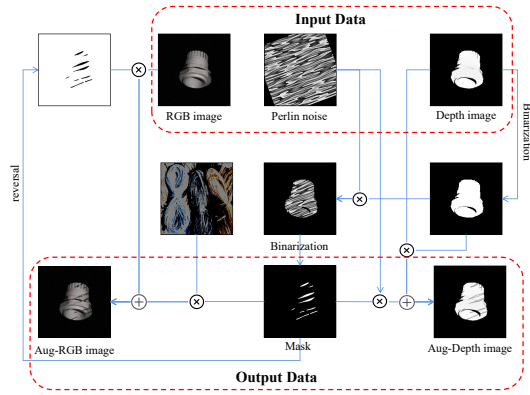


Figure 4: Illustration of anomaly generation processing.

Therefore, the final image reconstruction loss function should be:

$$\begin{aligned}
 L_{rec}(I, I_r) &= L_{rec}^{RGB}(I, I_r) + L_{rec}^{depth}(I, I_r) \\
 &= \lambda_1 L_{SSIM}^{RGB}(I, I_r) + \lambda_2 L_2^{RGB}(I, I_r) + \lambda_3 L_2^{depth}(I, I_r),
 \end{aligned} \quad (2)$$

where $\lambda_1, \lambda_2, \lambda_3$ are loss balancing hyper-parameters, All are set to 1 in our experimental setting.

3.2.2 Multi-modality Segmentation Network (MSN). The MSN evaluates the normality of each time slot (H, W). Similar to DRAEM [39], the training set samples are processed by the simulator and the discriminator performs mask identification by identifying the input of enhanced images and reconstructed images. EasyNet extracts multi-layer features evaluated by discriminators through an MRN. MSN utilizes multi-layer reconstruction features and enhanced image features, which come from our assumption that some features that deviate from the normal distribution will be removed gradually with the deepening of the multi-modality reconstruction network. By comparing the difference of eigenvalues before and after removal, the locations of outliers can be obtained.

When extracting reconstruction features and enhancing image features of multiple layers, we mainly adopt the first three layers of shallow networks of MRN and the last three layers of reconstructed features and carry out up-sampling operations to adapt for features of multiple layers. Moreover, we conduct ablation experiments. As shown in Section 4.2.4, experiments show that when two-layer features are adopted, both the accuracy and computing cost of the network are optimized. We use a two-layer multilayer perceptron structure (MLP) to process multi-layer scale features extracted from

RGB and depth images respectively. Finally, we use another two-layer MLP structure to combine the features of the two modes and perform positive and negative discriminations for each pixel in the image. As shown in Section 4.2, the proposed straightforward strategy is successful in reaching its goal.

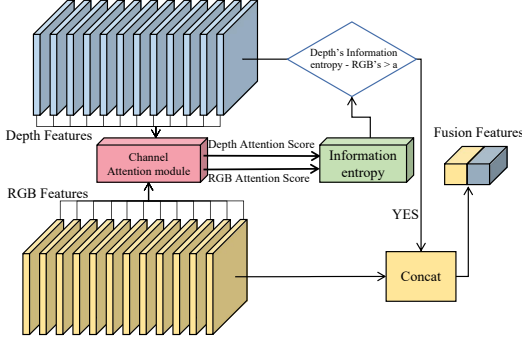


Figure 5: Illustration of information entropy scheme.

3.2.3 Attention-based Information Fusion Module. As noted in Section 3.1, exceptions may occur solely in pure RGB or depth images, or both. The combination of both features may diminish the overall performance of AD, where blending RGB and depth led to an inverse outcome. To address this issue, as shown in Figure 5, we generate multi-channel self-attention scores from input features in the input layer of MSN’s multi-layer perception module. We then compare the information entropy of the channel that integrates RGB and depth features with that of the channel integrating only pure RGB features. We hypothesize that the greater the information entropy of the channel attention score, the richer the feature knowledge it contains. If fusion features enhance the information gain beyond RGB features, it could have a positive effect on the performance of the results. The experimental results presented in Section 4.2.3 provide support for our theory. The mathematical representation of this process is shown in Formula 3.

$$F_{fusion} = \begin{cases} F_{RGB} + F_{depth}, & f_{IE}(F_{RGB} + F_{depth}) > f_{IE}(F_{RGB}) + \alpha \\ F_{RGB}, & f_{IE}(F_{RGB} + F_{depth}) \leq f_{IE}(F_{RGB}) + \alpha \end{cases} \quad (3)$$

where F_{fusion} represents the features after fusion, F_{RGB} represents the features of RGB, F_{depth} represents the features of depth, $f_{IE}(\cdot)$ represents the function of calculating information entropy, and α represents the threshold adjustment factor.

When calculating the loss between the predicted mask and the ground truth mask, we use the Focal Loss [22] function, which could well solve the problem of sample imbalance in the single-class classification of pixels. The formula is expressed as shown in Formula 4:

$$L_{focal}(M, M_{out}) = -\alpha_t (1 - p_t)^\gamma \log(p_t), \quad (4)$$

where α_t is a scaling factor related to class t , γ is an adjustable parameter, p_t corresponds to the predicted classification of pixel points, the abnormal category is 1, and the normal category is 0.

3.2.4 Total Loss Function. To sum up, training losses of networks mainly come from MRN and MSN. The main optimization objectives and tasks are reconstruction losses and classification losses. Finally, the overall loss of the network during training is as follows:

$$\begin{aligned} L_{total}(I, I_r) &= L_{rec}^{RGB}(I, I_r) + L_{rec}^{depth}(I, I_r) + L_{focal}(M, M_{out}) \\ &= \lambda_1 L_{SSIM}^{RGB}(I, I_r) + \lambda_2 L_2^{RGB}(I, I_r) \\ &\quad + \lambda_3 L_2^{depth}(I, I_r) + \lambda_4 L_{focal}(M, M_{out}), \end{aligned} \quad (5)$$

where $\lambda_1, \lambda_2, \lambda_3$, and λ_4 are loss balancing hyper-parameters. Easynet aims to meet the objectives of optimizing anomaly detection and reconstruction tasks while training, so we expect to optimize the above objectives by assigning weights to different losses. All four λ are set to 1 in our experimental setting.

3.2.5 Algorithms. The EasyNet is implemented as Algorithm 1. Firstly, images I_{rgb} and I_{depth} are enhanced by an anomaly generator Φ_{ag} to produce augmented images Aug_{rgb} and Aug_{depth} respectively. The reconstruction network Φ_{rec} then extracts depth and RGB features at different scales from these augmented images and origin images. Finally, network Φ_{seg} generates an anomaly score maps M and M_{rgb} corresponding to the original images. Additionally, the function Φ_{ai} generates corresponding self-attention information entropy scores for both RGB and RGB-D channels. To achieve optimal fusion information effect, both reconstruction loss and classification loss are calculated, followed by returning the loss gradient. this process allows the network to learn how to better combine RGB and depth features in a complementary and informative way.

4 EXPERIMENTS

4.1 Experimental Details

4.1.1 Datasets. MVTEC 3D-AD [6] includes ten categories and a total of 2,656 training samples along with 1,137 testing samples. The 3D scans in this dataset were acquired via a structured-light-powered industrial scanner that captured the x, y, and z coordinates of the target object. Additionally, RGB data is also collected at the same time for each point in the cloud. To process the 3D data accurately, it is crucial to remove all the background noise. A RANSAC algorithm is employed to estimate the background plane, ensuring that points within 0.005 distances were eliminated without disturbing the RGB data. However, their corresponding pixels in the RGB image were set to zero. This step minimized disturbances while enhancing the accuracy of anomaly detection.

Eyecandies [8] is a novel synthetic dataset comprising ten different categories of candies rendered in a controlled environment. Bonfiglioli *et al.* [9] generated item instances through modeling software and collected relevant data. The data set provides depth and RGB images in an industrial conveyor scenario. The ten categories of candies show different challenges, such as complex textures, self-occlusions, and specularities. By controlling the lighting conditions and parameters of a procedural rendering pipeline in the modeling software, the authors of the dataset produced datasets containing complex instances with varying conditions. Similar to MVTEC 3D-AD, the training dataset only consists of normal samples, while the testing dataset consists of normal and abnormal samples.

Table 1: I-AUROC score for anomaly detection of all categories of MVTec-3D AD.

Method	Bagel	Cable Gland	Carrot	Cookie	Dowel	Foam	Peach	Potato	Rope	Tire	Mean	Memory Bank Usage	Pre-trained Model Usage	
Pure Depth	Depth GAN [6]	0.530	0.376	0.607	0.603	0.497	0.484	0.595	0.489	0.536	0.521	0.523		
	Depth AE [6]	0.468	0.731	0.497	0.673	0.534	0.417	0.485	0.549	0.564	0.546	0.546		
	Depth VM [6]	0.510	0.542	0.469	0.576	0.609	0.699	0.450	0.419	0.668	0.520	0.546		
	Voxel GAN [6]	0.383	0.623	0.474	0.639	0.564	0.409	0.617	0.427	0.663	0.577	0.537		
	Voxel AE [6]	0.693	0.425	0.515	0.790	0.494	0.558	0.537	0.484	0.639	0.583	0.571		
	Voxel VM [6]	0.750	0.747	0.613	0.738	0.823	0.693	0.679	0.652	0.609	0.690	0.699		
	3D-ST [7]	0.862	0.484	0.832	0.894	0.848	0.663	0.763	0.687	0.958	0.486	0.748		
	PatchCore+FPFH [18]	0.825	0.551	0.952	0.797	0.883	0.582	0.758	0.889	0.929	0.653	0.782	✓	✓
	AST [30]	0.881	0.576	0.965	0.957	0.679	0.797	0.990	0.915	0.956	0.611	0.833	✓	✓
	M3DM [33]	0.941	0.651	0.965	0.969	0.905	0.760	0.880	0.974	0.926	0.765	0.874	✓	✓
	EasyNet(ours)	0.735	0.678	0.747	0.864	0.719	0.716	0.713	0.725	0.885	0.687	0.747		
	Pure RGB	DifferNet [27]	0.859	0.703	0.643	0.435	0.797	0.790	0.787	0.643	0.715	0.590	0.696	✓
PADiM [12]		0.975	0.775	0.698	0.582	0.959	0.663	0.858	0.535	0.832	0.760	0.764	✓	✓
PatchCore [25]		0.876	0.880	0.791	0.682	0.912	0.701	0.695	0.618	0.841	0.702	0.770	✓	✓
STEPM [32]		0.930	0.847	0.890	0.575	0.947	0.766	0.710	0.598	0.965	0.701	0.793	✓	✓
CS-Flow [16]		0.941	0.930	0.827	0.795	0.990	0.886	0.731	0.471	0.986	0.745	0.830	✓	✓
AST [30]		0.947	0.928	0.851	0.825	0.981	0.951	0.895	0.613	0.992	0.821	0.880	✓	✓
M3DM [33]		0.944	0.918	0.896	0.749	0.959	0.767	0.919	0.648	0.938	0.767	0.850	✓	✓
SPADE [11]		0.771	0.793	0.760	0.531	0.848	0.683	0.646	0.460	0.879	0.502	0.687	✓	✓
FastFlow [38]		0.624	0.472	0.654	0.694	0.501	0.667	0.595	0.632	0.816	0.731	0.639	✓	✓
RD4AD [14]		0.975	0.987	0.943	0.575	0.999	0.830	0.863	0.618	0.984	0.899	0.867	✓	✓
STPM [32]		0.899	0.706	0.796	0.486	0.512	0.678	0.502	0.666	0.962	0.581	0.679	✓	✓
EasyNet(ours)		0.982	0.992	0.917	0.953	0.919	0.923	0.840	0.785	0.986	0.742	0.904		
RGB+Depth	Depth GAN [6]	0.538	0.372	0.580	0.603	0.430	0.534	0.642	0.601	0.443	0.577	0.532		
	Depth AE [6]	0.648	0.502	0.650	0.488	0.805	0.522	0.712	0.529	0.540	0.552	0.595		
	Depth VM [6]	0.513	0.551	0.477	0.581	0.617	0.716	0.450	0.421	0.598	0.623	0.555		
	Voxel GAN [6]	0.680	0.324	0.565	0.399	0.497	0.482	0.566	0.579	0.601	0.482	0.517		
	Voxel AE [6]	0.510	0.540	0.384	0.693	0.446	0.632	0.550	0.494	0.721	0.413	0.538		
	Voxel VM [6]	0.553	0.772	0.484	0.701	0.751	0.578	0.480	0.466	0.689	0.611	0.609		
	3D-ST [7]	0.950	0.483	0.986	0.921	0.905	0.632	0.945	0.988	0.976	0.542	0.833		
	PatchCore+FPFH [18]	0.918	0.748	0.967	0.883	0.932	0.582	0.896	0.912	0.921	0.886	0.865	✓	✓
	AST [30]	0.983	0.873	0.976	0.971	0.932	0.885	0.974	0.981	1.000	0.797	0.937	✓	✓
	M3DM [33]	0.994	0.909	0.972	0.976	0.960	0.942	0.973	0.899	0.972	0.850	0.945	✓	✓
	EasyNet(ours)	0.991	0.998	0.918	0.968	0.945	0.945	0.905	0.807	0.994	0.793	0.926		

4.1.2 Evaluation Metrics. Due to the unsupervised experimental setting, accuracy is usually not used to evaluate the performance of anomaly detection methods, but rather the Area Under the Curve (AUC) metric, we use the I-AUROC and P-AUROC in our method. Besides, the common evaluation metrics we used include Area Under the Receiver Operating Characteristic Curve (AUROC) and the Area Under the Precision-Recall curve (AUPR/AP), and the explanation of I-AUROC and P-AUROC please refer to the *supplementary materials*.

4.1.3 Implementation Details. This section presents the implementation details of our experiments.

MRN uses the "UNet-like" structure as the primary network with intermediate skip operations subtracted primarily from the original UNet. The input image is resized to 256×256 , and the abnormal and normal images are allocated according to a 1:1 ratio. The abnormal images are applied with Berlin noise [40] added on top of normal images. For MSN, the two-layer MLP network is used to fuse different scale features of RGB and depth features. In experiment 4.2.3, the two layers MLPs network are employed to fuse different modal features. The input and output features of all the MLPs have the same size of 256×256 . And a SE block [19] is utilized for Attention-based Information Fusion Scheme to score channel attention for both modes.

The training process adopted the Adam optimizer with a learning rate of 0.002, which is dynamically adjusted twice, at $0.8 \times$ epochs and $0.9 \times$ epochs, with a multiplier factor of 0.2. The batch size is set to 8. Finally, we report the best anomaly detection results obtained after 800 training steps of MRN.

4.2 Experimental Results and Analysis

4.2.1 RGB+Depth on MVTec 3D-AD and Eyescandies. Table 1 and Table 2 clearly demonstrate that EasyNet achieves the state-of-the-art performance on MVTec 3D-AD and Eyescandies without using pre-trained model and memory bank. Specifically, EasyNet outperforms AutoEncoder [9] and PatchCore+FPFH [18] in RGB+Depth setting of Eyescandies by a large margin, 20.7% and 6.9%, respectively. Even though PatchCore+FPFH [18] uses large pre-trained models, i.e., WideResNet-50 and huge memory banks for the features of each point, it still cannot compete with EasyNet. For MVTec 3D-AD, AST [30] and M3DM [33] are the cutting-edge models in MVTec 3D-AD. However, both of them use large pre-trained models or memory banks. In specific, M3DM uses two pre-trained models (Point Transformer and Vision Transformer) to extract the features from depth images and RGB images. In addition, M3DM employs two large memory banks (average 6.098 GB) to store the features from depth images and RGB images. Due to strict storage limitations in practice, M3DM cannot be perfectly fit in real-world applications.

Table 2: I-AUROC score for anomaly detection of all categories of Eyescandies.

Method		Candy Cane	Chocolate Cookie	Chocolate Cookie	Confetto	Gummy Bear	Hazelnut Truffle	Licorice Sandwich	Lollipop	Marshmallow	Peppermint Candy	Mean	Memory Bank usage	Pre-trained Model Usage
Pure Depth	Raw [18]	0.654	0.510	0.563	0.451	0.433	0.454	0.472	0.515	0.626	0.366	0.504	✓	
	HoG [18]	0.653	0.510	0.470	0.723	0.728	0.520	0.717	0.667	0.699	0.742	0.643	✓	
	SIFT [18]	0.589	0.582	0.683	0.885	0.663	0.480	0.778	0.702	0.746	0.790	0.690	✓	
	FPFH [18]	0.670	0.710	0.805	0.806	0.748	0.515	0.794	0.757	0.765	0.757	0.733	✓	
	EasyNet(ours)	0.629	0.716	0.768	0.731	0.660	0.710	0.712	0.711	0.688	0.731	0.706		
Pure RGB	GANomaly [3]	0.485	0.512	0.532	0.504	0.558	0.486	0.467	0.511	0.481	0.528	0.507		
	DFKDE [2]	0.539	0.577	0.482	0.548	0.541	0.492	0.524	0.602	0.658	0.591	0.555		✓
	DFM [1]	0.532	0.776	0.624	0.675	0.681	0.596	0.685	0.618	0.964	0.770	0.692		✓
	STEPM [32]	0.551	0.654	0.576	0.784	0.737	0.790	0.778	0.620	0.840	0.749	0.708		✓
	PaDiM [12]	0.531	0.816	0.821	0.856	0.826	0.727	0.784	0.665	0.987	0.924	0.794	✓	✓
	AutoEncoder [9]	0.527	0.848	0.772	0.734	0.590	0.508	0.693	0.760	0.851	0.730	0.701		
	EasyNet(ours)	0.723	0.925	0.849	0.966	0.705	0.815	0.806	0.851	0.975	0.960	0.858		
RGB+Depth	AutoEncoder [9]	0.529	0.861	0.739	0.752	0.594	0.498	0.679	0.651	0.838	0.750	0.689		
	PatchCore+FPFH [18]	0.606	0.904	0.792	0.939	0.720	0.563	0.867	0.860	0.992	0.842	0.809	✓	✓
	EasyNet(ours)	0.737	0.934	0.866	0.966	0.717	0.822	0.847	0.863	0.977	0.960	0.869		

Table 3: Ablation studies on attention-based information entropy fusion module. The best is in red and the second best is in blue.

MVTec 3D-AD	Evaluation	Bagel	Cable gland	Carrot	Cookie	Dowel	Foam	Peach	Potato	Rope	Tire	Mean
	Gate Close	0.982	0.992	0.917	0.953	0.919	0.923	0.840	0.785	0.986	0.742	0.904
	Gate Open	0.974	0.996	0.914	0.968	0.941	0.938	0.882	0.781	0.982	0.793	0.917
	Gate Control	0.991	0.998	0.918	0.968	0.945	0.945	0.905	0.807	0.994	0.793	0.926
Eyescandies	Evaluation	Candy Cane	Chocolate Cookie	Chocolate Cookie	Confetto	Gummy Bear	Hazelnut Truffle	Licorice Sandwich	Lollipop	Marshmallow	Peppermint Candy	Mean
	Gate Close	0.723	0.925	0.849	0.966	0.705	0.815	0.806	0.851	0.975	0.960	0.857
	Gate Open	0.722	0.919	0.827	0.945	0.685	0.813	0.846	0.850	0.975	0.959	0.854
	Gate Control	0.737	0.934	0.866	0.966	0.717	0.822	0.847	0.863	0.977	0.960	0.869

Table 4: The ablation study for the number of fusion layers. The best is in red and the second best is in blue.

RGB+Depth	Evaluation	Bagel	Cable gland	Carrot	Cookie	Dowel	Foam	Peach	Potato	Rope	Tire	Mean
Image AUC	1 layer	0.967	0.981	0.912	0.890	0.901	0.908	0.763	0.717	1.000	0.731	0.877
	2 layers	0.974	0.996	0.914	0.968	0.941	0.938	0.882	0.781	0.982	0.793	0.917
	3 layers	0.964	1.000	0.884	0.889	0.967	0.932	0.734	0.697	1.000	0.866	0.893
Image AP	1 layer	0.992	0.995	0.982	0.969	0.976	0.975	0.915	0.873	1.000	0.906	0.958
	2 layers	0.994	0.999	0.981	0.991	0.984	0.984	0.966	0.930	0.992	0.927	0.975
	3 layers	0.991	1.000	0.975	0.966	0.992	0.982	0.903	0.916	1.000	0.963	0.969
Pixel AUC	1 layer	0.875	0.861	0.963	0.678	0.716	0.998	0.969	0.921	0.928	0.861	0.877
	2 layers	0.935	0.941	0.971	0.897	0.885	0.997	0.992	0.888	0.955	0.728	0.919
	3 layers	0.904	0.717	0.836	0.651	0.809	0.997	0.914	0.942	0.986	0.97	0.873
Pixel AP	1 layer	0.020	0.025	0.097	0.015	0.026	0.803	0.081	0.032	0.133	0.163	0.139
	2 layers	0.039	0.062	0.188	0.025	0.034	0.562	0.298	0.034	0.144	0.031	0.142
	3 layers	0.041	0.043	0.084	0.008	0.121	0.648	0.017	0.014	0.249	0.134	0.136

Although PatchCore+FPFH has a relatively small memory footprint (249.260 MB on average), the actual performance is not as good as EasyNet. The memory bank size of M3DM and PatchCore+FPFH on the MVTec 3D-AD can be found in *supplementary materials*. AST also adopts two EfficientNet-B5 as the feature extractor for depth image and RGB image, which violate the storage limitation in IM. Moreover, according to Table 5, massive usage of pre-trained models will slow down the inference speed, which cannot meet the requirement of IM. Furthermore, the performance gap among EasyNet, AST and M3DM is very small, 2.1% and 1.2%. Hence, EasyNet is the best 3D-AD model to meet all the demands of IM.

4.2.2 Pure RGB Performance. In real-world applications, the limitation of the depth sensor is very large since the effective distance range of depth sensor is 3 meters. In addition, most of the depth sensors are easily affected by the lighting condition. Hence, as for

simulating the failure of the depth sensor, we conduct the experiment by only using RGB images as the input. In pure RGB branch of Table 1 and Table 2, EasyNet achieves state-of-the-art performance in I-AUROC in pure RGB track. In specific, EasyNet outperforms in pure RGB of Eyescandies with a large margin, 15.7% to AutoEncoder [9] and 6.4% to PaDiM [12]. Moreover, EasyNet gets 5.97% better I-AUROC score than M3DM and 2.65% better I-AUROC score than AST. In total, The performance of EasyNet is robust even though the depth sensor is a failure.

4.2.3 Attention-based Information Entropy Fusion Module. Table 3 clearly illustrates the effectiveness of our proposed attention-based information entropy fusion module in EasyNet. The gate network is the key to control multi-feature fusion. We conduct the ablation studies on three options, Gate Close, Gate Open and Gate Control, respectively. Gate Close means that EasyNet only utilizes RGB

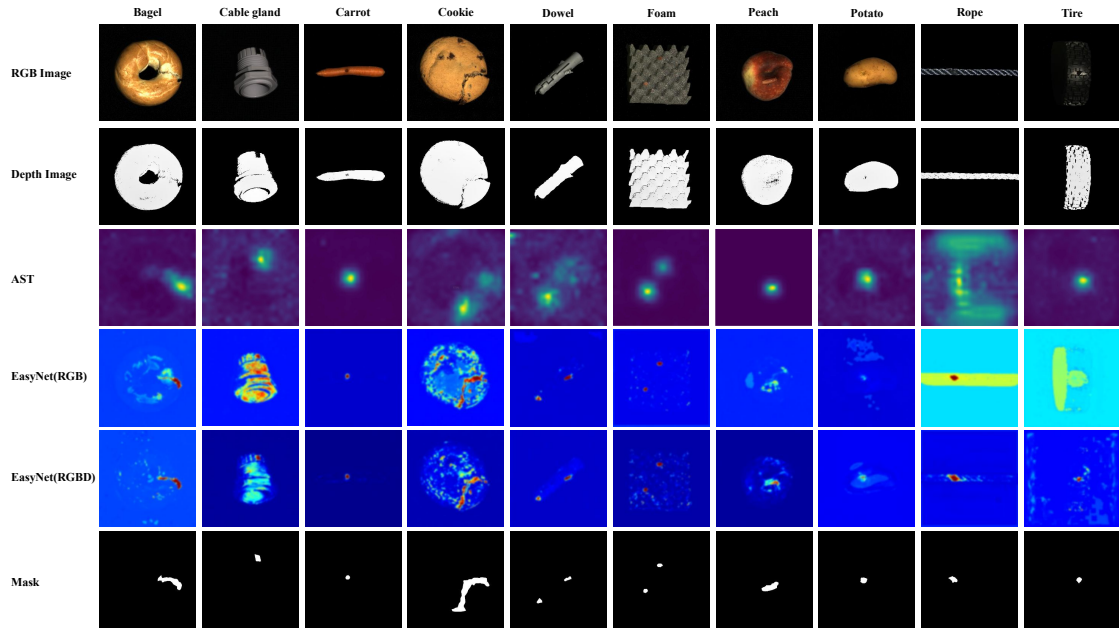


Figure 6: Visualizations on MVTec 3D-AD, which are obtained by AST [30], EasyNet (RGB) and EasyNet (RGB-D), respectively.

images as the input and ignores depth information. Gate Open denotes that EasyNet uses both the RGB image and the depth image and combines their features for evaluation. Gate Control means that EasyNet adopts an attention-based information entropy fusion module to select the depth features during the inference case. In Gate Open, we discover that depth information degrades the total performance if we select both RGB features and depth features during inference. In some case, we find that only utilizing RGB features are enough to detect the anomalies. Then the depth information may work as the noise to interfere with the final result. Therefore, we design an attention-based information entropy fusion module to select the feature for fusion, which can enhance the performance of all classes in MVTec 3D-AD and Eyescandies.

4.2.4 Ablation study on the number of fusion layers. As described in Section 3.2.2, the MSN is utilized for segmenting outliers by fusing multi-layer enhanced image features and reconstructed ones. Table 4 presents that EasyNet performs optimally when incorporating features from only two layers. Specifically, the performance metrics of I-AUROC and P-AUROC are respectively improved by 4.36% and 4.57% with two layers compared to one layer; and they are further increased by 2.62% and 5.27% with three layers compared to one layer. These results indicate that the employment of two feature layers can achieve the best performance both in anomaly detection and localization. In contrast, using three feature layers leads to performance degradation, which verifies our hypothesis. The deepening of the multi-modality reconstruction network can gradually eliminate some abnormal feature parts, whereas using three feature layers introduces more feature removal of abnormal parts, thereby leading to poor discriminator performance.

4.2.5 Accuracy VS Inference Speed. As we previously described in Section 1, inference speed is one of the important factors to be considered in IM. Since the real production line needs

to check each product in real time. Table 5 shows EasyNet obtains the fastest speed among the cutting-edge anomaly detection methods but without sacrificing the performance. In specific, EasyNet gets 125% FPS better than AST and 93900% FPS than M3DM. As for performance, the performance gap among EasyNet, AST and M3DM is very small, 2.1% and 1.2%. Therefore, EasyNet is the most deployment-friendly 3D-AD method for IM.

Table 5: Inference abilities.

Method	I-AUROC	FPS
BTF [17]	0.865	27.92
AST [30]	0.937	41.94
M3DM [33]	0.945	0.10
EasyNet(ours)	0.926	94.55

4.3 Visualization

Figure 6 visualizes the performance of EasyNet on MVTec 3D-AD, demonstrating the effectiveness of the proposed method. In Figure 6, Compared to existing 3D anomaly detection methods (AST [30]), EasyNet can reduce false positive rates significantly and achieve higher segmentation accuracy. Furthermore, the fusion method reduces false positives for anomalies such as *cable glands*, compared to using only RGB images. Abnormalities in *peach* and *potato* are also more clearly visible on depth graphs, indicating the importance of using depth image information in industrial AD. In addition, EasyNet is not affected by domain gap between natural and industrial images and has a higher inference speed than existing methods. Note that we put the visualization results of EasyNet on Eyescandies in *supplementary materials*.

Algorithm 1 EasyNet pseudo-code

```

1: Input: train dataloader  $D_{train}$ , test dataloader  $D_{test}$ , epochs
2: Output: trained  $\Phi_{rec}$  and  $\Phi_{seg}$ ,  $M$ 
3: Initialization randomly:  $\Phi_{rec}$  and  $\Phi_{seg}$ 
4: /*Training time*/
5: for  $i = 0$  to epochs do
6:   for  $I_{rgb}, I_{depth}, M_{gt} \leftarrow D_{train}$  do
7:      $Aug_{rgb}, Aug_{depth} = \Phi_{ag}(I_{rgb}, I_{depth})$ 
8:      $F_{rgb}, F_{depth}, Rec_{rgb}, Rec_{depth} = \Phi_{rec}(Aug_{rgb}, Aug_{depth})$ 
9:      $F_{fusion} = Concat(F_{rgb}, F_{depth})$ 
10:     $M_{rgb} = \Phi_{seg}(F_{rgb})$ 
11:     $M = \Phi_{seg}(F_{fusion})$ 
12:     $L_{rgb} = \Phi_{loss}(Aug_{rgb}, Aug_{depth}, I_{rgb}, I_{depth}, M_{rgb}, M_{gt})$ 
13:     $L_{total} = \Phi_{loss}(Aug_{rgb}, Aug_{depth}, I_{rgb}, I_{depth}, M, M_{gt})$ 
14:     $L_{rgb}.backward$ 
15:     $L_{total}.backward$ 
16:   end for
17: end for
18: /*Inference time*/
19: for  $I_{rgb}, I_{depth}, M_{gt} \leftarrow D_{test}$  do
20:    $Aug_{rgb}, Aug_{depth} = \Phi_{ag}(I_{rgb}, I_{depth})$ 
21:    $F_{rgb}, F_{depth}, Rec_{rgb}, Rec_{depth} = \Phi_{rec}(Aug_{rgb}, Aug_{depth})$ 
22:    $S_{rgb} = \Phi_{ai}(Feature_{rgb})$ 
23:    $S_{fusion} = \Phi_{ai}(F_{rgb}, F_{depth})$ 
24:   if  $S_{fusion} - S_{rgb} > \alpha$  then
25:      $F_{fusion} = Concat(F_{rgb}, F_{depth})$ 
26:   else
27:      $F_{fusion} = F_{rgb}$ 
28:   end if
29:    $M = \Phi_{seg}(F_{fusion})$ 
30:   return  $M$ 
31: end for

```

5 CONCLUSIONS

This paper addresses a promising and challenging task, i.e., deployment-friendly 3D-AD and proposes an easy but effective neural network (termed as EasyNet) to achieve competitive performance without using large pre-trained models and memory banks. Specifically, as for getting rid of large pre-trained models and memory banks, EasyNet employs MRN to implicitly detect and reconstruct the anomalies with semantically plausible anomaly-free content, while keeping the non-anomalous regions of the input image unchanged. Meanwhile, EasyNet proposes an MSN to produce an accurate anomaly segmentation map from the concatenated reconstructed RGB images and depth images and their original appearances. In the test phase, EasyNet adopts multi-head self-query scores in the early fusion stage to select the informative depth features before fusing with RGB features. To this end, EasyNet achieves the fastest inference speed without sacrificing performance.

REFERENCES

- [1] Nilesh A. Ahuja, Ibrahim J. Ndiour, Trushant Kalyanpur, and Omesh Tickoo. 2019. Probabilistic Modeling of Deep Features for Out-of-Distribution and Adversarial Detection. *ArXiv abs/1909.11786* (2019).
- [2] Samet Akcay, Dick Ameln, Ashwin Vaidya, Barath Lakshmanan, Nilesh Ahuja, and Utku Genc. 2022. Anomalib: A Deep Learning Library for Anomaly Detection. *arXiv:2202.08341* [cs.CV]
- [3] Samet Akcay, Amir Atapour-Abarghouei, and T. Breckon. 2018. GANomaly: Semi-Supervised Anomaly Detection via Adversarial Training. In *Asian Conference on Computer Vision*.
- [4] Paul Bergmann, Michael Fauser, David Sattlegger, and Carsten Steger. 2019. MVTEC AD—A comprehensive real-world dataset for unsupervised anomaly detection. *Proceedings of the IEEE/CVF conference on computer vision and pattern recognition* (2019), 9592–9600.
- [5] Paul Bergmann, Michael Fauser, David Sattlegger, and Carsten Steger. 2020. Uninformed students: Student-teacher anomaly detection with discriminative latent embeddings. *Proceedings of the IEEE/CVF Conference on Computer Vision and Pattern Recognition* (2020), 4183–4192.
- [6] Paul Bergmann, Xin Jin, David Sattlegger, and Carsten Steger. 2021. The MVTEC 3D-AD Dataset for Unsupervised 3D Anomaly Detection and Localization. *ArXiv abs/2112.09045* (2021).
- [7] Paul Bergmann and David Sattlegger. 2022. Anomaly Detection in 3D Point Clouds using Deep Geometric Descriptors. *2023 IEEE/CVF Winter Conference on Applications of Computer Vision (WACV)* (2022), 2612–2622.
- [8] Luca Bonfiglioli, Marco Toschi, Davide Silvestri, Nicola Fioraio, and Daniele De Gregorio. 2022. The Eyecandies Dataset for Unsupervised Multimodal Anomaly Detection and Localization. *Proceedings of the Asian Conference on Computer Vision* (2022), 3586–3602.
- [9] Luca Bonfiglioli, Marco Toschi, Davide Silvestri, Nicola Fioraio, and Daniele De Gregorio. 2022. The Eyecandies Dataset for Unsupervised Multimodal Anomaly Detection and Localization. In *Asian Conference on Computer Vision*.
- [10] Yunkang Cao, Xiaohao Xu, and Weiming Shen. 2023. Complementary Pseudo Multimodal Feature for Point Cloud Anomaly Detection. *arXiv preprint arXiv:2303.13194* (2023).
- [11] Niv Cohen and Yedid Hoshen. 2020. Sub-Image Anomaly Detection with Deep Pyramid Correspondences. *ArXiv abs/2005.02357* (2020).
- [12] Thomas Defard, Aleksandr Setkov, Angélique Loesch, and Romaric Audigier. 2020. PaDiM: a Patch Distribution Modeling Framework for Anomaly Detection and Localization. In *ICPR Workshops*.
- [13] Thomas Defard, Aleksandr Setkov, Angélique Loesch, and Romaric Audigier. 2021. Padim: a patch distribution modeling framework for anomaly detection and localization. *International Conference on Pattern Recognition* (2021), 475–489.
- [14] Hanqiu Deng and Xingyu Li. 2022. Anomaly Detection via Reverse Distillation from One-Class Embedding. *2022 IEEE/CVF Conference on Computer Vision and Pattern Recognition (CVPR)* (2022), 9727–9736.
- [15] Denis Gudovskiy, Shun Ishizaka, and Kazuki Kozuka. 2022. Cflow-ad: Real-time unsupervised anomaly detection with localization via conditional normalizing flows. *Proceedings of the IEEE/CVF Winter Conference on Applications of Computer Vision* (2022), 98–107.
- [16] Denis A. Gudovskiy, Shun Ishizaka, and Kazuki Kozuka. 2021. CFLOW-AD: Real-Time Unsupervised Anomaly Detection with Localization via Conditional Normalizing Flows. *2022 IEEE/CVF Winter Conference on Applications of Computer Vision (WACV)* (2021), 1819–1828.
- [17] Eliahu Horwitz and Yedid Hoshen. 2022. Back to the feature: classical 3d features are (almost) all you need for 3d anomaly detection. *arXiv preprint arXiv:2203.05550* (2022).
- [18] Eliahu Horwitz and Yedid Hoshen. 2022. An Empirical Investigation of 3D Anomaly Detection and Segmentation. *ArXiv abs/2203.05550* (2022).
- [19] Jie Hu, Li Shen, Samuel Albanie, Gang Sun, and Enhua Wu. 2017. Squeeze-and-Excitation Networks. *IEEE Transactions on Pattern Analysis and Machine Intelligence* 42 (2017), 2011–2023.
- [20] Chun-Liang Li, Kihyuk Sohn, Jinsung Yoon, and Tomas Pfister. 2021. Cutpaste: Self-supervised learning for anomaly detection and localization. *Proceedings of the IEEE/CVF Conference on Computer Vision and Pattern Recognition* (2021), 9664–9674.
- [21] Wujin Li, Jiawei Zhan, Jinbao Wang, Bizhong Xia, Bin-Bin Gao, Jun Liu, Chengjie Wang, and Feng Zheng. 2022. Towards Continual Adaptation in Industrial Anomaly Detection. *Proceedings of the 30th ACM International Conference on Multimedia* (2022), 2871–2880.
- [22] Tsung-Yi Lin, Priya Goyal, Ross B. Girshick, Kaiming He, and Piotr Dollár. 2017. Focal Loss for Dense Object Detection. *2017 IEEE International Conference on Computer Vision (ICCV)* (2017), 2999–3007.
- [23] Jiaqi Liu, Guoyang Xie, Jingbao Wang, Shangnian Li, Chengjie Wang, Feng Zheng, and Yaochu Jin. 2023. Deep Industrial Image Anomaly Detection: A Survey. *arXiv:2301.11514* [cs.CV]
- [24] Zhikang Liu, Yiming Zhou, Yuansheng Xu, and Zilei Wang. 2023. SimpleNet: A Simple Network for Image Anomaly Detection and Localization. *arXiv preprint arXiv:2303.15140* (2023).
- [25] Karsten Roth, Latha Pemula, Joaquin Zepeda, Bernhard Schölkopf, Thomas Brox, and Peter Gehler. 2021. Towards Total Recall in Industrial Anomaly Detection. *2022 IEEE/CVF Conference on Computer Vision and Pattern Recognition (CVPR)* (2021), 14298–14308.
- [26] Karsten Roth, Latha Pemula, Joaquin Zepeda, Bernhard Schölkopf, Thomas Brox, and Peter Gehler. 2022. Towards total recall in industrial anomaly detection. *Proceedings of the IEEE/CVF Conference on Computer Vision and Pattern Recognition*

- (2022), 14318–14328.
- [27] Marco Rudolph, Bastian Wandt, and Bodo Rosenhahn. 2020. Same Same But DifferNet: Semi-Supervised Defect Detection with Normalizing Flows. *2021 IEEE Winter Conference on Applications of Computer Vision (WACV)* (2020), 1906–1915.
- [28] Marco Rudolph, Bastian Wandt, and Bodo Rosenhahn. 2021. Same same but differnet: Semi-supervised defect detection with normalizing flows. *Proceedings of the IEEE/CVF winter conference on applications of computer vision* (2021), 1907–1916.
- [29] Marco Rudolph, Tom Wehrbein, Bodo Rosenhahn, and Bastian Wandt. 2022. Asymmetric Student-Teacher Networks for Industrial Anomaly Detection. *2023 IEEE/CVF Winter Conference on Applications of Computer Vision (WACV)* (2022), 2591–2601.
- [30] Marco Rudolph, Tom Wehrbein, Bodo Rosenhahn, and Bastian Wandt. 2022. Asymmetric Student-Teacher Networks for Industrial Anomaly Detection. *arXiv preprint arXiv:2210.07829* (2022).
- [31] Hannah M Schlüter, Jeremy Tan, Benjamin Hou, and Bernhard Kainz. 2022. Natural Synthetic Anomalies for Self-supervised Anomaly Detection and Localization. *European Conference on Computer Vision* (2022), 474–489.
- [32] Guodong Wang, Shumin Han, Errui Ding, and Di Huang. 2021. Student-Teacher Feature Pyramid Matching for Anomaly Detection. In *British Machine Vision Conference*.
- [33] Yue Wang, Jinlong Peng, Jiangning Zhang, Ran Yi, Yabiao Wang, and Chengjie Wang. 2023. Multimodal Industrial Anomaly Detection via Hybrid Fusion. *ArXiv abs/2303.00601* (2023).
- [34] Zhou Wang, Alan Conrad Bovik, Hamid R. Sheikh, and Eero P. Simoncelli. 2004. Image quality assessment: from error visibility to structural similarity. *IEEE Transactions on Image Processing* 13 (2004), 600–612.
- [35] Guoyang Xie, Jinbao Wang, Jiaqi Liu, Yaochu Jin, and Feng Zheng. 2023. Pushing the Limits of Fewshot Anomaly Detection in Industry Vision: Graphcore. In *The Eleventh International Conference on Learning Representations*. <https://openreview.net/forum?id=xzmqxHdZAwO>
- [36] Guoyang Xie, Jinbao Wang, Jiaqi Liu, Jiayi Lyu, Y. Liu, Chengjie Wang, Feng Zheng, and Yaochu Jin. 2023. IM-IAD: Industrial Image Anomaly Detection Benchmark in Manufacturing. *ArXiv abs/2301.13359* (2023).
- [37] Zhiyuan You, Lei Cui, Yujun Shen, Kai Yang, Xin Lu, Yu Zheng, and Xinyi Le. 2022. A Unified Model for Multi-class Anomaly Detection. *arXiv preprint arXiv:2206.03687* (2022).
- [38] Jiawei Yu1, Ye Zheng, Xiang Wang, Wei Li, Yushuang Wu, Rui Zhao, and Liwei Wu. 2021. FastFlow: Unsupervised Anomaly Detection and Localization via 2D Normalizing Flows. *ArXiv abs/2111.07677* (2021).
- [39] Vitjan Zavrtnik, Matej Kristan, and Danijel Skočaj. 2021. Draem-a discriminatively trained reconstruction embedding for surface anomaly detection. *Proceedings of the IEEE/CVF International Conference on Computer Vision* (2021), 8330–8339.
- [40] Vitjan Zavrtnik, Matej Kristan, and Danijel Skočaj. 2021. DRAEM – A discriminatively trained reconstruction embedding for surface anomaly detection. *2021 IEEE/CVF International Conference on Computer Vision (ICCV)* (2021), 8310–8319.
- [41] Vitjan Zavrtnik, Matej Kristan, and Danijel Skočaj. 2022. DSR–A dual subspace re-projection network for surface anomaly detection. *arXiv preprint arXiv:2208.01521* (2022).